

# Using Transfer Functions to Quantify ENSO Dynamics in Data and Models

BY DOUGLAS G. MACMYNOWSKI<sup>1</sup> AND ELI TZIPERMAN<sup>2</sup>

<sup>1</sup>*Control & Dynamical Systems, California Institute of Technology*

<sup>2</sup>*Dept of Earth & Planetary Sciences and School of Engineering and Applied Sciences, Harvard University*

Transfer function tools commonly used in engineering control analysis can be used to better understand the dynamics of ENSO, compare data with models, and identify systematic model errors. The transfer function describes the frequency-dependent input-output relationship between any pair of causally-related variables, and can be estimated from time series. This can then be used to diagnose the underlying differential equations that relate the variables, and hence to describe the dynamics of individual subsystem processes that are relevant to the overall dynamics of ENSO. Estimating process parameters allows the identification of compensating model errors that may lead to a seemingly realistic simulation for the wrong reason. This tool is illustrated here using the TAO array for ocean data, the GFDL CM2.1 general circulation model (GCM), and the Cane-Zebiak ENSO model. The delayed oscillator description of ENSO is used to motivate a few of the relevant processes involved in the dynamics, although any other ENSO mechanism could be used instead. We identify several differences in the processes between the models and data that may be useful in improving the models. The same methodology may also be useful in understanding the dynamics and evaluating models of other climate processes.

**Keywords:** ENSO, feedbacks, transfer functions, control

## 1. Introduction

The dynamics of ENSO are not consistently well captured in GCMs (AchutaRao & Sperber, 2006; Collins & The CMIP Modeling Groups, 2005; van Oldenborgh *et al.*, 2005). Furthermore, even if the output statistics (period, amplitude, etc.) are reasonably well simulated, there is no guarantee that there are no compensating errors in the model that lead to seemingly good results for the wrong reason. As a result, even if the present climate is well simulated, it does not guarantee that changes in the dynamics with climate change will be correctly captured. It is thus important to evaluate models at an *individual process* level, rather than being satisfied with matching general output metrics. The same issue of compensating model errors is relevant in any aspect of climate dynamics, e.g., for understanding multi-decadal variability of ENSO, variability of the NAO, Atlantic meridional overturning circulation and more. This issue is not restricted to climate variability modes, and models that fit the observed global warming record of the 20th century diverge in both prediction mode (Meehl *et al.*, 2007) and in trying to simulate the Atlantic

MOC during the last glacial maximum, for example (Otto-Bliesner *et al.*, 2007). This again indicates the possibility of compensating errors and requires model validation by process rather than by output metrics such as the globally averaged surface temperature.

In a recent paper (MacMynowski & Tziperman, 2010) we introduced the *transfer function* as an additional tool for estimating the process dynamics of ENSO. Here we extend the previous results to consider additional processes involved in ENSO dynamics, and provide more detail on the transfer function estimation, and error bounds in particular.

The term “transfer function” is taken from the control engineering literature (e.g., Astrom & Murray, 2008), and refers to a frequency-dependent input-output relationship between any pair of causally related variables. The transfer function can be derived from the underlying differential equation relating the input and output variables. Alternatively, identifying the transfer function from data or model time series of the input and output variables can be used both to verify the differential equation, and to estimate values for unknown parameters. In MacMynowski & Tziperman (2010), we considered two examples. First, the western boundary reflection coefficient relating westward-propagating Rossby waves and the reflected eastward-propagating Kelvin waves; this relationship was considered as there are ample existing estimates to compare our results with. And second, the relationship between eastern Pacific sea surface temperature (SST) anomaly (NINO3 index) and arriving Kelvin waves in the eastern Pacific. These relationships were compared for TAO data from ocean buoys (McPhaden *et al.*, 1998), model output from the GFDL CM2.1 coupled GCM (Wittenberg *et al.*, 2006; van Oldenborgh *et al.*, 2005), and the Cane-Zebiak model of ENSO (Zebiak & Cane, 1987). The analysis reveals compensating errors in the GFDL model, where SST response to Kelvin waves is too large, compensated by too large a dissipation. The errors in the Cane-Zebiak model are found to be larger (see also Wittenberg, 2002).

The two input-output relationships already considered in MacMynowski & Tziperman (2010) illustrate the utility of the transfer function analysis, and the importance of estimating process dynamics, but they do not give a complete picture of ENSO dynamics. Here we present the transfer functions for a total of six processes which span the entire delayed oscillator feedback loop (Suarez & Schopf, 1988; Battisti, 1988) shown in Fig. 1. Each block in this figure represents a process (that is, relationship between variables) for which the amplitude will be estimated from appropriate model and data time series in Sec. 3. We present and analyze the six transfer functions for both TAO array observations and two models. Other descriptions of ENSO dynamics, such as the recharge-oscillator of Jin (1997), could similarly be used to motivate input-output relationships relevant to understanding differences between models and data.

The transfer function approach represents an additional tool that may be useful in diagnosing process dynamics, which can complement other approaches; see a summary in Guilyardi *et al.* (2009b); Collins *et al.* (2010), and analysis of specific processes in, for example, (Capotondi *et al.*, 2006; Dewitte *et al.*, 2007; Guilyardi *et al.*, 2009a; Lloyd *et al.*, 2009).

Transfer functions are also expected to be useful in identifying compensating model errors in studies of other climate variability modes and climate change and we have made the needed code available on our web pages. The next section introduces



where  $s = 2\pi if$  and  $\hat{T}(s)\hat{K}_e^*(s)$  may be interpreted as a cross correlation between the temperature and Kelvin wave amplitude in spectral space. The transfer function thus depends on frequency according to the differential operator in the relation between the input and output.

The frequency-dependent transfer function can also be estimated from time series of the input and output (e.g., Section 6.2, Swanson, 2000). Given input and output time series  $x(t)$  and  $y(t)$  and their Fourier transforms  $\hat{x}(f)$  and  $\hat{y}(f)$ , (2.3) suggests that the transfer function can be estimated as the ratio of cross-correlation to the auto-correlation in frequency space,

$$T_{xy}(f) = \frac{\langle \hat{x}(f)\hat{y}^*(f) \rangle}{\langle \hat{x}(f)\hat{x}^*(f) \rangle} = \frac{S_{xy}(f)}{S_{xx}(f)}, \quad (2.4)$$

The auto- and cross-correlations  $S_{xx}(f)$  and  $S_{xy}(f)$  are estimated by (i) dividing the time series for  $x$  and  $y$  into  $n$  possibly overlapping segments of smaller length,  $x_k(t)$  and  $y_k(t)$ ; (ii) computing the Fourier transforms  $\hat{x}_k(f)$ ,  $\hat{y}_k(f)$  of each of the windowed signals  $x_k(t)$ ,  $y_k(t)$  in the  $k$ th segment and calculating their products in each segment; and (iii) averaging these products over the segments to calculate the correlations in Fourier space in order to eliminate the uncorrelated parts of the response,

$$S_{xy}(f) = \frac{1}{n} \sum_{k=1}^n \hat{x}_k(f)\hat{y}_k^*(f). \quad (2.5)$$

The transfer function is, in general, complex and both its magnitude and phase,  $\Phi(f)$ , provide useful information,

$$T_{xy}(f) = |T_{xy}(f)|e^{i\Phi(f)}. \quad (2.6)$$

With sufficient averaging, the contribution due to any part of the output signal that is not correlated with the input signal will tend to zero, yielding an estimate due only to the correlated component. However, increasing the averaging by increasing the number of segments results in shorter segments and thus smaller resolved frequency range. Because ‘‘windowing’’ (gradual tapering of the time series near their ends) is required on each data segment to avoid the implicit discontinuity at the segment boundary, non-zero overlaps between segments can be used to increase the number of averages without creating information that was not present in the original data; see Welch (1967) for a more detailed discussion. Here we typically use two-year data segments; this means that  $1/(2 \text{ years})$  is the lowest frequency resolved. We apply a Hamming window on each segment, and use a segment overlap of 50% (i.e., using years 0–2, 1–3, 2–4, etc.).

The magnitude of the error in  $T_{xy}(f)$  that results from contributions to the output signal not correlated with the input signal, can be estimated from the coherence,

$$\gamma_{xy}^2(f) = \frac{|S_{xy}(f)|^2}{S_{xx}(f)S_{yy}(f)}, \quad (2.7)$$

which estimates the fraction of the output variance that is correlated with the input. The standard deviation of the estimation error in the transfer function magnitude

and phase (eq. 6.2.21 and 6.2.22, Swanson, 2000) can then be approximated as

$$\sigma_{|T_{xy}|}(f) \simeq \left( \frac{1}{2n} \frac{1 - \gamma_{xy}^2(f)}{\gamma_{xy}^2(f)} \right)^{1/2} |T_{xy}(f)|, \quad (2.8)$$

$$\sigma_{\Phi_{xy}}(f) \simeq \tan^{-1} \left[ \left( \frac{1}{2n} \frac{1 - \gamma_{xy}^2(f)}{\gamma_{xy}^2(f)} \right)^{1/2} \right], \quad (2.9)$$

where the approximation is valid for small errors. In practice, there is rarely sufficient data to make these errors negligible. Nonlinear effects in the relationship between input and output will also show up as noise, and reduced coherence. There are additional sources of uncertainty in the interpretation of the estimated transfer function. A correlation between  $x$  and  $y$  may be due to the input  $x$  affecting the output  $y$  (the presumed interpretation), a closed feedback loop where the output  $y$  affects the input  $x$ , or some independent factor affecting both  $x$  and  $y$ . As an example, consider western Pacific Rossby wave influencing the reflected Kelvin waves. A closed feedback loop effect exists because the reflected Kelvin waves, in turn, affect east Pacific SST, the SST influences winds, which in turn excite Rossby waves again. An independent factor affecting both input and output could be western Pacific wind anomalies that simultaneously excite both Kelvin and Rossby waves, biasing the estimate of western boundary reflection coefficient. The phase of the transfer function can be useful in diagnosing these factors, by noting which signal leads the other, or whether the two signals are in phase.

As an example of critically evaluating a transfer function estimate, consider the following system, modified from (2.1) by the addition of an uncorrelated unknown noise process  $\nu(t)$  that affects both the input  $H$  and the output  $y(t)$  which are related as follows,

$$\dot{T} = \mu H - \epsilon T + \nu, \quad y = T + \nu, \quad (2.10)$$

where we set  $\mu = 1$  and  $\epsilon = 4$  (years<sup>-1</sup>). Assume that the input  $H$  is a known random Markov process with an auto correlation time four times larger than the time constant  $\epsilon^{-1}$ , and that  $\nu$  is white noise, which therefore dominates the response at high frequencies. The transfer function is shown in Fig. 2, including its magnitude and phase estimates (with error bars indicating two standard deviations). Two different estimates are plotted, based on averaging over 2-year segments, and 4-year segments. The latter gives increased frequency resolution, particularly apparent at low frequencies, but as can be seen in the left panel, does not necessarily lead to improved estimates of the parameters  $\mu$  and  $\epsilon$  because there are fewer averages used in constructing the transfer function estimate at each frequency.

As an example of how the transfer function phase may be used to critically evaluate the results, note that with  $\nu = 0$  the phase corresponding to (2.10) should be  $-90^\circ$  at high frequencies. This is because our equations reduce in the absence of noise to  $\dot{y} = \mu H - \epsilon y$ . In Fourier space this becomes  $if\hat{y} = \mu\hat{H} - \epsilon\hat{y}$ , and for high frequency, where  $f \gg \epsilon$ , this may be approximated as  $if\hat{y} \approx \mu\hat{H}$ , and the factor  $i = e^{\pi/2}$  implying a  $90^\circ$  phase difference between the input  $H$  and output  $y$ . However, introducing the noise results both in high uncertainty at high frequencies and an average phase closer to  $0^\circ$ , indicating that the output at these frequencies is not dominated by the dynamics governed by  $\mu$  and  $\epsilon$  in (2.10). Thus the transfer

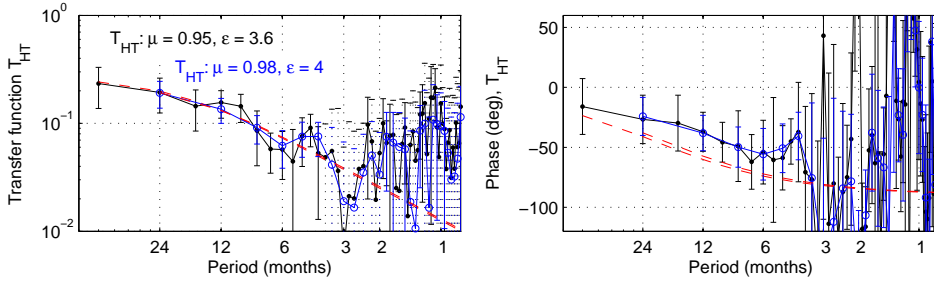


Figure 2. Transfer function estimated from simulated data for (2.10), showing transfer function magnitude (left), and phase (right). The total 20-year record is divided into either 2-year (blue) or 4-year (black) time intervals, corresponding to 19 or 9 averages (with 50% overlap). Red dashed lines show the optimal fit of the magnitude, and the corresponding phase, to the transfer function  $\mu/(s + \epsilon)$  corresponding to (2.10), and the best fit parameter values are shown on the magnitude plot. The two red lines in each panel correspond to a fit based on the 2 year and 4 year segments. Despite the higher frequency resolution, more accurate parameter estimates are obtained with the shorter time records due to the increased averaging. Simulation parameters are chosen to give coherence comparable to the real data for  $T_{KT}$  (see Fig. 4(b).)

function phase indicates that the transfer function estimate is not reliable at high frequencies.

This example demonstrates how estimating the transfer function at each frequency is immediately useful in understanding the underlying differential equation that relates the variables. The transfer function estimates can also be used to estimate the parameters of the differential equation, e.g.,  $\mu$  and  $\epsilon$  in (2.10). In principle these parameters could be identified directly from the time domain data either using least-squares in the case of fitting a constant relationship, or by fitting an AR model. However, if some fraction of the frequency range is dominated by noise (as in the above example at high frequencies) or by other processes, this problem would bias the time-domain estimate. Such a problem should be immediately apparent in the transfer function frequency response, and can be taken into account in deciding which frequency range to use for fitting parameters.

The fit of model parameters such as  $\mu$  and  $\epsilon$  in the above example requires careful treatment as well. Consider first the case where the assumed transfer function is a constant  $\alpha$  over frequency, and we are trying to fit its value. Then the best estimate of the constant  $\alpha$  can be obtained from a weighted least-squares, using the variance (2.8) to weight the quality of the transfer function information  $T_{xy}(f)$  at each frequency,

$$\alpha = \frac{\sum_i \sigma_{xy}^{-2}(f_i) |T_{xy}(f_i)|}{\sum_i \sigma_{xy}^{-2}(f_i)}. \quad (2.11)$$

Note that if the relationship involves a time-delay, then the phase will vary with frequency, and the magnitude of the relationship is better estimated from just the magnitude of the transfer function, rather than from its complex value.

The more general case of a frequency-dependent fit is illustrated by the transfer function (2.3). Fitting the squared magnitude of the transfer function, then the

data at all  $N$  frequencies are related to the unknown parameters  $\mu$  and  $\epsilon$  by,

$$\begin{bmatrix} 1 & -|T_{xy}(f_1)|^2 \\ \vdots & \vdots \\ 1 & -|T_{xy}(f_N)|^2 \end{bmatrix} \begin{bmatrix} \mu^2 \\ \epsilon^2 \end{bmatrix} = \begin{bmatrix} (2\pi f_1)^2 |T_{xy}(f_1)|^2 \\ \vdots \\ (2\pi f_N)^2 |T_{xy}(f_N)|^2 \end{bmatrix}. \quad (2.12)$$

These equations can be solved using weighted least squares to estimate  $\mu$  and  $\epsilon$ , where each measurement (information at each frequency  $f_i$ ) is weighted by the inverse of its variance. This algorithm is used to obtain the fits in Fig. 2 and in the following analysis of ENSO models and observations.

### 3. Application to ENSO

#### (a) Choice of transfer functions to evaluate

The first step in using transfer functions to diagnose the dynamics is to define appropriate input/ output variable pairs. Returning now to the schematic representation in Fig. 1, define the following variables.

- $T$  as the SST averaged over the NINO3 region,
- $W_r$  and  $W_k$  as the central Pacific atmospheric wind stress projected onto the Kelvin and Rossby meridional structure (as in Boulanger & Menkes (1995)),
- $K_c, R_c$  as the central Pacific Kelvin and Rossby waves excited by wind anomalies,
- $K_w, R_w$  as the western Pacific Kelvin and Rossby wave amplitudes, and
- $K_e$  as the eastern Pacific Kelvin wave amplitude.

Fig. 1 can be used to motivate the following delay-differential-equation describing the dynamics of ENSO (Suarez & Schopf, 1988; Battisti, 1988),

$$\dot{T} = \alpha T - \beta T(t - \delta). \quad (3.1)$$

This yields an oscillatory response for the appropriate values of the delay and constants. However, implicit in obtaining Eq. (3.1) from Fig. 1 is the assumption that only the relationship between the eastern Pacific Kelvin wave and SST is prognostic, as in (2.1). All of the other input-output relationships are assumed diagnostic, such that their transfer functions are constants, independent of frequency. We will see that this is not quite true of the data, though it may be a reasonably good approximation.

The projection of data onto Kelvin and Rossby waves is done following Boulanger & Menkes (1995); Boulanger *et al.* (2003), using a single baroclinic mode based only on the layer thickness anomaly (and not currents) (Boulanger *et al.*, 2003). The atmospheric wind forcing on the Kelvin and Rossby waves is computed as in (eq. A7, Boulanger & Menkes, 1995). For TAO data, the wind stress is computed using the expression for friction velocity derived by Vera (unpublished manuscript, 1983) and published as (eq. 8, Large *et al.*, 1995).

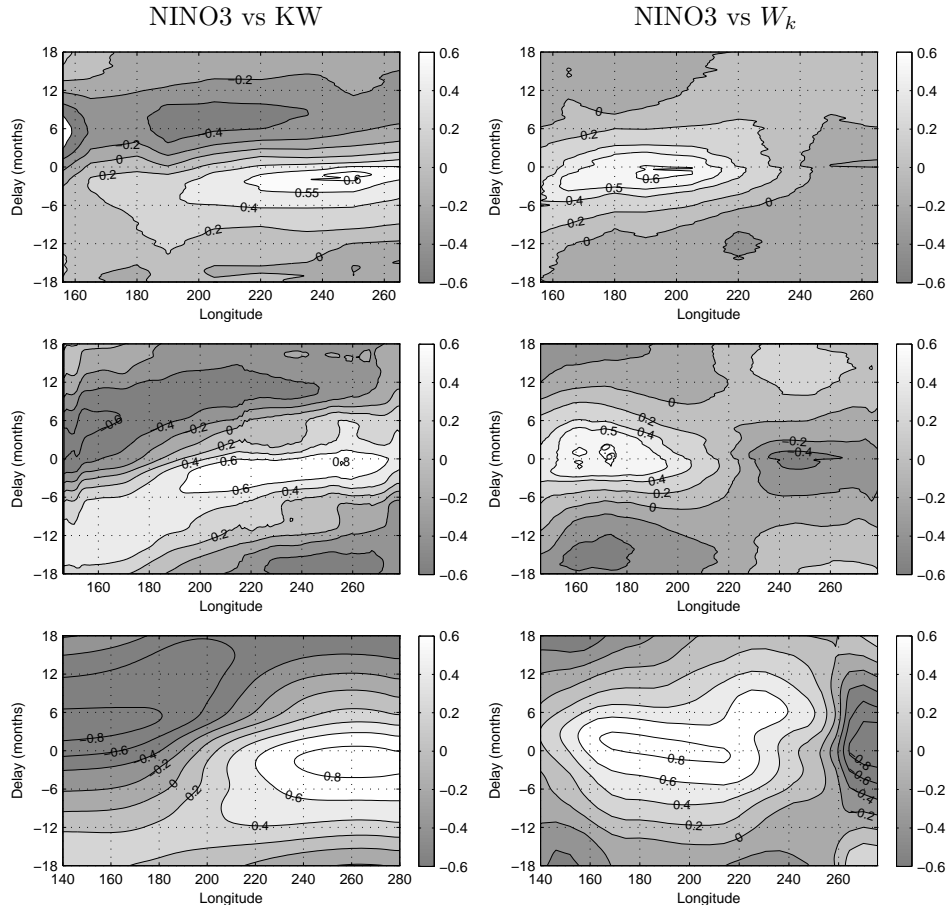


Figure 3. Correlation between NINO3 index and Kelvin wave amplitudes (left column) and between NINO3 and wind stress projected onto Kelvin wave meridional structure (right column). Upper plots are computed from TAO data, middle pair of plots are computed from GFDL model output, and lower pair of plots are computed from the CZ model. These plots are useful for understanding what longitude to use in evaluating transfer functions.

The appropriate longitude ranges of “east”, “central” and “west” (Fig. 1) can be chosen through correlation analysis, shown in Fig. 3 for each of the sources of data considered herein. Similar correlation plots have been used by Zelle *et al.* (2004) to estimate time delays.

The left columns of Fig. 3 show the maximum influence of Kelvin waves on NINO3 to occur east of  $240^\circ$ , while the right columns of Fig. 3 show most of the influence of NINO3 on creating Kelvin waves to be west of  $240^\circ$ . Hence this longitude can be used to understand the influence of Kelvin waves on SST without a confounding feedback influence of SST on Kelvin waves. The resulting transfer function is found to be not strongly dependent on the chosen longitude.

Similar correlation plots indicate that most of the influence of SST on the forcing of ocean wave modes occurs east of  $156^\circ$ . Thus this longitude can be used to evaluate the Rossby and Kelvin modes near the western boundary in order to calculate the

reflection coefficient  $T_{RK}$  without interference from the forcing of the waves by the atmospheric response to eastern Pacific SST. This longitude also has the advantage of being sufficiently removed from land masses close to the equator.

Finally, the peak excitation of winds by NINO3 is near  $180^\circ$  (in GFDL model) and  $190^\circ$  (in TAO data and CZ model), and the latter is therefore used in evaluating the corresponding transfer functions  $T_{TW_{k,r}}$  and  $T_{W_rR}$ ,  $T_{W_kK}$ . In order to estimate the effect of wind on the oceanic Kelvin wave directly, without a confounding influence from wind causing Rossby waves that reflect off the western boundary as Kelvin waves, it is necessary to subtract a delayed version of the western Pacific Kelvin wave from the central Pacific Kelvin before computing the transfer function  $T_{W_kK}$ .

(b) *Results for ENSO transfer function estimates*

Transfer function estimates for each of the blocks in Fig. 1 (a total of six different transfer functions) are computed from TAO data, GFDL model output, and CZ model output, and plotted in Figs. 4–6. Note that the western boundary reflection coefficient and  $T_{KT}$  (panels a and b of Figs. 4–6 were discussed in MacMynowski & Tziperman (2010), and are only briefly summarized here for completeness. Transfer function estimates, and the correlation estimates in Fig. 3, are based on weekly averaged TAO data from 1994–2009, 22 years of weekly averaged GFDL model output simulated under present-day conditions, and 75 years of CZ model output, all with the seasonal cycle removed. Note that the GFDL model captures the general features of ENSO reasonably well but with too high an amplitude and possibly too short a period (Wittenberg *et al.*, 2006). Because the time scale of the processes estimated here is short (weeks to a few months), 22 years of model output are sufficient to constrain these transfer functions even if calculating ENSO event statistics generally requires a longer record (Wittenberg, 2009).

Consider first the TAO array estimates. The western boundary reflection coefficient is reasonably constant at low frequencies; the higher frequency content in Fig. 4a (and Fig. 5a) is due to correlated excitation of Kelvin and Rossby waves from wind disturbances MacMynowski & Tziperman (2010). This can be verified from the roughly constant phase at higher frequencies (Fig. 7), rather than the linearly increasing phase with frequency expected from a time delay. The magnitude of the reflection coefficient is consistent with other estimates, e.g., 0.33–0.37 in Boulanger *et al.* (2003). Also described in MacMynowski & Tziperman (2010), the excitation of SST due to eastern Pacific Kelvin wave anomalies is consistent with (2.1), validating the form of the underlying dynamics for this process. Fitting the transfer function yields estimates for both the feedback strength  $\mu$  in (2.1) and the dissipation  $\epsilon$ ; these are indicated on the figure.

The transfer function describing the forcing by east Pacific SST, of wind anomalies projected on the Rossby and Kelvin modes,  $T_{TW_{k,r}}$ , are given in panels (c) and (d) of Figs. 4–6 and show that NINO3 anomalies produce a roughly proportional wind-stress anomaly (i.e., independent of frequency). This is consistent with the short atmospheric response time of a few days.

However, an interesting result we obtain here is that the forcing of ocean waves from applied wind perturbations ( $T_{W_kK}$  and  $T_{W_rR}$ , panels (e) and (f)) does involve some frequency dependence, indicating a prognostic relationship between the

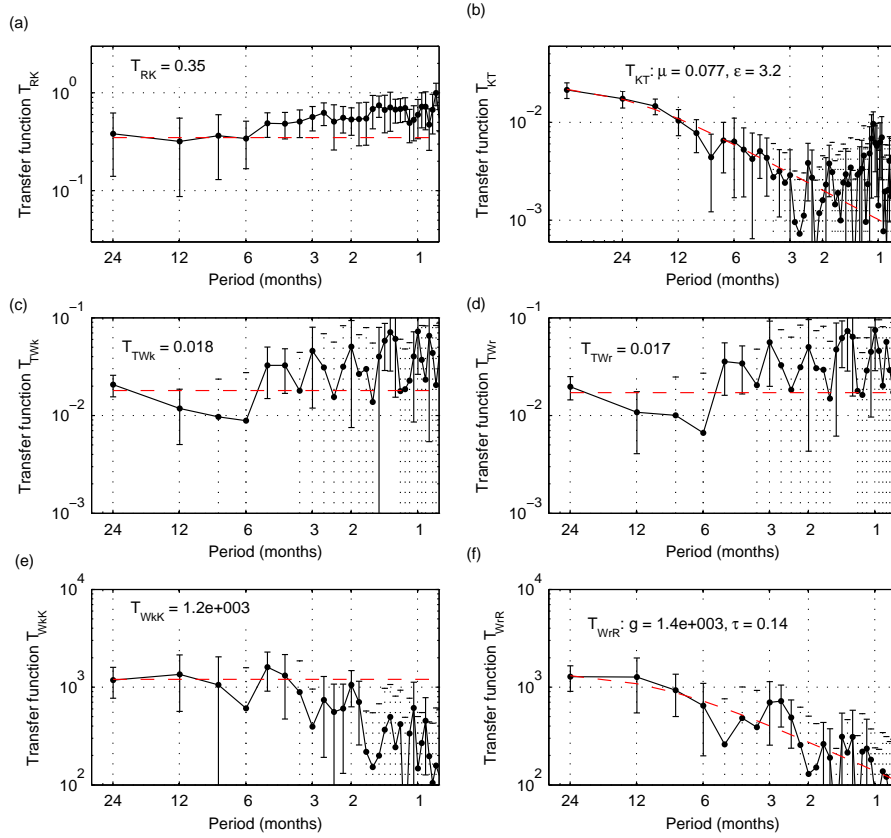


Figure 4. Transfer functions evaluated from TAO data, including error bars computed from coherence, and the optimal fit to the low frequency behavior. (a) from the western Pacific Rossby wave to the western Pacific Kelvin (reflection coefficient), (b) from the eastern Pacific Kelvin wave to SST response (NINO-3 index), (c) from NINO-3 to the central Pacific wind stress projected onto the Kelvin mode shape, (d) from NINO-3 to the central Pacific wind stress projected onto the Rossby mode shape, (e) from mid-Pacific wind stress projected onto Kelvin, to the amplitude of the resulting eastern Pacific Kelvin wave, and (f) from mid-Pacific wind stress projected onto Rossby, to the amplitude of the resulting western Pacific Rossby wave.

two which is normally ignored in the ENSO literature. The system responds more strongly to low-frequency perturbations than to high frequencies. This frequency dependence suggests (see examples in section 2) a first-order differential equation  $\tau dR/dt = gW_r - R$  and therefore transfer function  $T_{RW_r} = g(1 + \tau s)^{-1}$ . The time constant  $\tau$  weighting the time derivative term for generating Rossby waves is estimated to be  $\sim 1.7$  months and is fast enough that it may be a reasonable approximation to ignore it in simple heuristic models of ENSO such as the delayed oscillator. However, based on the transfer function shape we can predict that the low frequency relationship between the wind and the forced Rossby waves will be underestimated if the time series (involving the full frequency content of the signal)

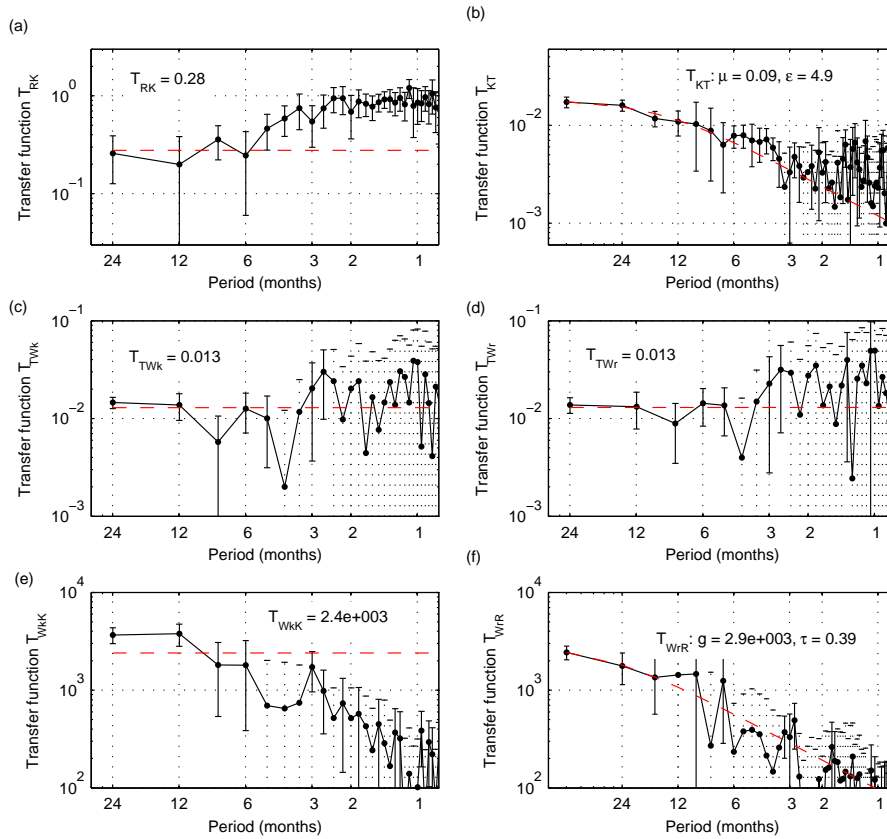


Figure 5. Transfer functions evaluated from GFDL model; cases (a)-(f) as in Fig. 4.

is used to naively estimate the value of an assumed frequency-independent relationship between the wind and the forced Rossby waves. The time constant involved in generating Kelvin waves is shorter and difficult to reliably estimate from this data (and also from GFDL model output).

As noted in MacMynowski & Tziperman (2010), the GFDL model has slightly too low a reflection coefficient (this is not expected to be dominant in ENSO dynamics (e.g. Boulanger *et al.*, 2003), and small compensating errors in the excitation of NINO3 perturbations from Kelvin wave anomalies, with both the strength of the response and the dissipation being slightly too high. Additional compensating errors are found in the transfer functions considered here for the first time: we find that the GFDL model simulates a too weak wind stress response to NINO3 anomalies (transfer functions  $T_{TW_{k,r}}$ , Fig. 5(c) and (d)). This is again compensated by another error of the model wind stress having too large an effect on ocean waves (transfer functions  $T_{W_kK}$  and  $T_{W_{fR}}$ , Fig. 5(e) and (f)). The inertia effect in wave excitation (that is, the time constant  $\tau$  in  $T_{W_{fR}}$  in particular) also seems to be too strong, with high frequency perturbations resulting in a smaller ocean response than the corresponding process estimated from data. The time constant weighting

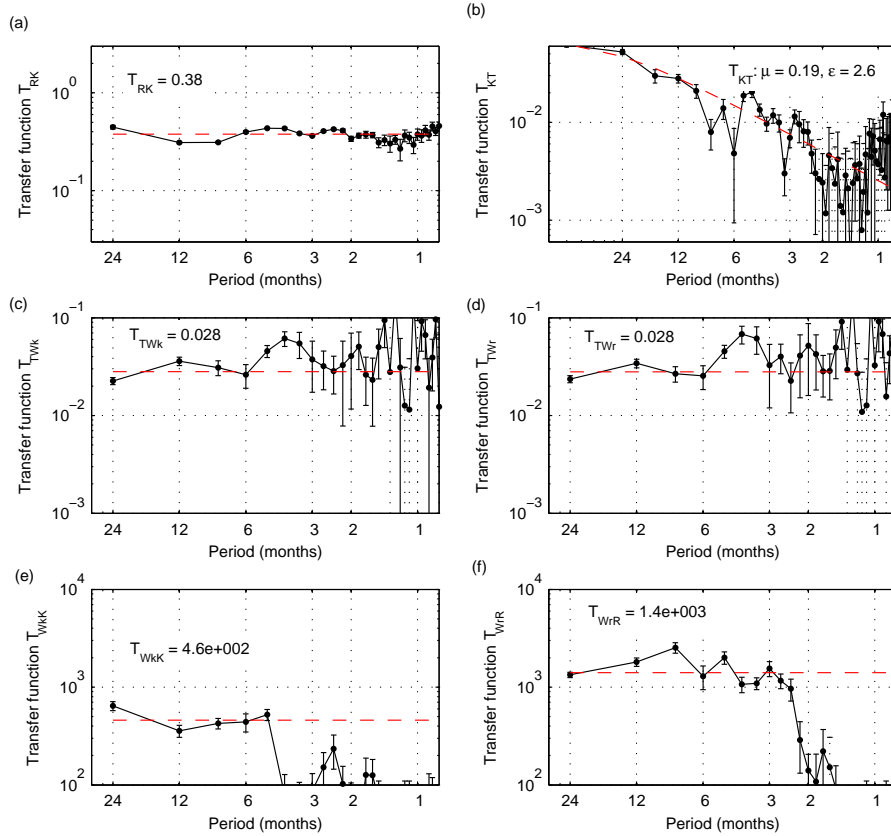


Figure 6. Transfer functions evaluated from CZ model, using baseline parameters; cases (a)-(f) as in Fig. 4. Note that the error bars are much smaller here than in Figs. 4 and 5 due to the longer time series used in estimating the transfer functions.

the corresponding time derivative term is uncertain from the GFDL model output but estimated to be  $\sim 5$  months, a factor of 3 larger than is estimated from the TAO data (4-year data segments are useful here to estimate the time constant).

None of these process discrepancies correspond directly to individual parameters that can be modified in the GCM. However, understanding errors in individual processes is still invaluable in tuning the model to improve the simulation of ENSO.

The CZ model western boundary reflection coefficient is specified in the model, and MacMynowski & Tziperman (2010) showed, encouragingly, that the transfer function analysis yields close to the correct value of a theoretical perfect reflection of 0.41 (Fig. 6(a)). The NINO3 response to Kelvin wave (thermocline) anomalies in the CZ model is more than a factor of two too large. The ability to tune parameters in this model to improve the match between model and data is illustrated in MacMynowski & Tziperman (2010), where both the advective and thermocline feedbacks are retuned in the model to improve the match of this process transfer function with data.

We find here, in addition, that the excitation of wind stress due to NINO3

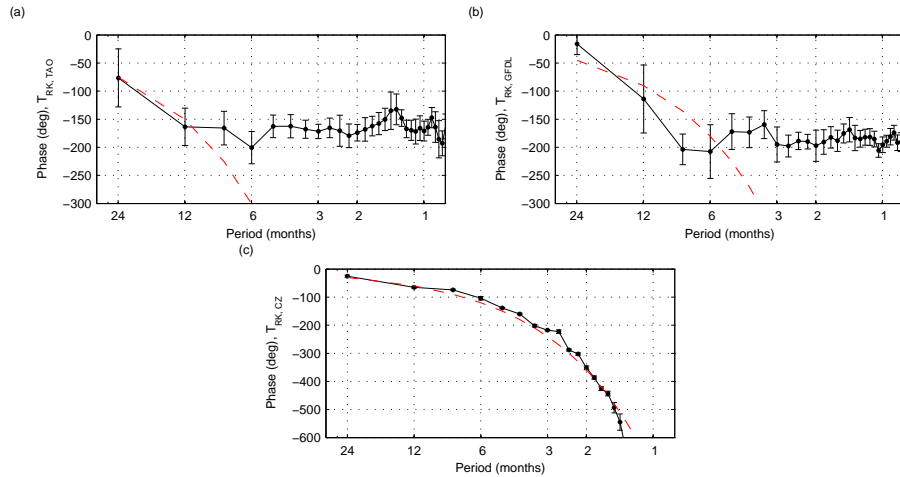


Figure 7. Phase of the transfer function from western Pacific Rossby wave to western Pacific Kelvin wave (the western boundary reflection coefficient) evaluated from (a) TAO data, (b) GFDL model output, and (c) CZ model output. The dashed red lines correspond to a linearly increasing phase with frequency due to a time delay of 5, 3, or 2 months respectively. The CZ model has no external forcing, and reflection is the only mechanism for generating western Pacific Kelvin waves. For both the data and the GFDL model, the anti-correlated Kelvin and Rossby wave amplitudes for frequencies higher than (1/year) seem dominated by other processes such as western Pacific wind forcing rather than by the reflection process. The lower frequency behavior, where the Kelvin wave has a physical phase-lag relative to the Rossby, results from a reflection process.

anomalies in the CZ model is also significantly larger than the corresponding processes in observations. The excitation of Rossby waves by winds (transfer function  $T_{W_r,R}$ , Fig. 6(f)) has a moderate error, so that the excitation of Rossby waves due to NINO3 anomalies is a factor of 1.5 larger than in data (product  $T_{TW_r} \times T_{W_r,R}$ ). There is an even more significant error in capturing the amplitude of the Kelvin wave response to wind stress anomalies ( $T_{W_k,K}$ , Fig. 6(e)). Because this process amplitude is too small, the Kelvin waves forced by NINO3 anomalies are slightly too weak rather than too large. Overall, the product of the three transfer functions involved in the eastern Pacific feedback ( $T_{KT} \times T_{TW_k} \times T_{W_k,K}$ , together corresponding to the parameter  $\alpha$  in (3.1)) is again a factor of 1.5 larger than in TAO data. This is a significant difference, indicating the need for model tuning, and can be diagnosed thank to the transfer function tools employed in this analysis.

Finally, the phase of the transfer functions also provides most useful information, often allowing us to evaluate the reliability of the amplitude estimate. An example is shown in Fig. 7 for the phase of the transfer function between western Pacific Rossby waves and Kelvin waves, corresponding to the western boundary reflection coefficient. Note that the waves are estimated at some distance away from the boundary and therefore one expects some delay between the arriving Rossby waves and the reflected kelvin waves. In general, the input-output relationship may therefore be written as  $KW(t) = a \times RW(t - \tau)$ . Taking the Fourier transform, the

transfer function is  $T_{xy}(s) = ae^{-i2\pi f\tau}$  which has an amplitude equal to the reflection coefficient  $a$ , and a phase increasing linearly with frequency,  $\phi_{xy}(f) = -2\pi\tau f$ . This clearly fits the transfer function from Rossby to Kelvin wave evaluated from the CZ model in Fig. 7(c), with a time-delay of two months corresponding to the wave propagation delay from  $156^\circ\text{W}$  where the waves are estimated, to the western boundary ( $124^\circ$  in this model) and back. Note that the frequency axis is plotted on a log scale, hence the phase does not show as a straight line. As noted earlier, the corresponding transfer functions evaluated from either TAO data or the GFDL model output show a constant phase at higher frequencies (Figs. 7(a) and (b)), indicating that there is no time delay between the signals at these frequencies, and suggesting that something other than wave reflection is involved. One possibility is a simultaneous excitation of western Pacific Rossby and Kelvin waves by local wind perturbations, leading to the waves having the same phase. There is insufficient data at lower frequencies for the observations and GFDL model to confidently determine the time delay involved in the wave travel from the longitude where the waves are estimated to the western boundary and back. The apparently larger delays than in the CZ model may be due to the dominant reflection occurring further west than the CZ model boundary, differences in wave propagation speed, other physical processes that result in Kelvin waves, or simply insufficient data for a reliable estimate.

#### 4. Conclusions

Transfer functions are useful tools for understanding the dynamics of processes involved in ENSO, or potentially other aspects of climate variability. Using time series of input and output signals, we can identify frequency-domain relationships between them, and use this both to understand the underlying differential equations describing the dynamics, and to estimate parameters. Applying this to estimates of processes involved in ENSO using TAO data, the GFDL CM2.1 GCM model, and the CZ model, we are able to quantitatively compare different individual processes between the observations and models, and therefore identify several significant compensating errors in both models.

For the GFDL model, in addition to the compensating errors in the SST response to Kelvin wave (thermocline) anomalies that were identified in MacMynowski & Tziperman (2010), we also find differences between the model and data for processes involving the wind stress. The wind stress induced by SST changes is too weak, and this is compensated by too large an ocean wave response to a given wind stress perturbation. In addition, the response time involved in the ocean response to applied wind stress is significantly too large in the GFDL model. Note that for both the GFDL model and the analysis of TAO data, the Kelvin wave equilibrates to wind stress anomalies much faster than the Rossby wave. The time constants estimated from data are 1.7 months for the Rossby wave and roughly a factor of two faster for the Kelvin wave.

Using the original values for all CZ model parameters, the process errors in this model are found to be significantly larger than in the GCM examined here. The SST response to an arriving Kelvin wave is too strong, the wind stress anomalies that result from SST anomalies are also too strong, and there is some compensation from too small an ocean response to wind stress anomalies. All of these process

errors suggest that the seemingly realistic simulation of ENSO using the original CZ parameters is likely influenced by compensating errors, and perhaps not “correct” for the right reasons.

It is important to understand that the first and perhaps most crucial step in a transfer function analysis is the choice of input and output variables. Our choices were motivated by the delay oscillator mechanism. The advantage of the methodology is that if the choice is wrong (say because the delay oscillator mechanism has nothing to do with the dynamics of ENSO, and specifically Kelvin waves in the east Pacific do not affect the NINO3 SST), then one gets immediate indication of this in the results. That is, the transfer function will come out not significantly different from zero. Thus the method can not only be used to quantify individual processes, but also to find out if a given mechanism is consistent with the model output or observations. In our case, we do find that the transfer functions spanning the entire delay oscillator ENSO mechanism are significant, and thus that this mechanism is a viable approach to describing the ENSO cycle. This does not exclude additional effects or alternative descriptions such as the recharge oscillator (Jin, 1997) or others (Wang & Picaut, 2004; Weisberg & Wang, 1997). We are currently in the process of examining the transfer functions corresponding to some alternative descriptions of ENSO.

This analysis of ENSO models and observations here demonstrate that transfer function can be used to quantify individual physical processes in climate models in a way that allows the identification of model errors and compensating errors. Given that such compensating errors are a major concern for the reliability of model future predictions, we feel this tool can be used to study and improve climate models in general.

## Acknowledgments

We are grateful to Gabriel Vecchi for providing the GFDL model output. The ocean data were made available by the TAO Project Office of NOAA/PMEL. Funding for this work is from DOE grant DE-SC0004984. ET is also funded by the NSF climate dynamics program, grant ATM-0754332 and by the NASA ECCO-II project, and thanks the Weizmann institute for its hospitality during parts of this work.

## References

- AchutaRao, K. & Sperber, K. R. 2006 ENSO simulation in coupled ocean-atmosphere models: are the current models better? *Clim. Dyn.*, **27**, 1–15.
- Astrom, K. J. & Murray, R. M. 2008 *Feedback systems: An introduction for scientists and engineers*. Princeton University Press.
- Battisti, D. S. 1988 The dynamics and thermodynamics of a warming event in a coupled tropical atmosphere/ocean model. *J. Atmos. Sci.*, **45**, 2889–2919.
- Boulanger, J.-P., Cravatte, S. & Menkes, C. 2003 Reflected and locally wind-forced interannual equatorial Kelvin waves in the western Pacific Ocean. *J. Geophysical Research*, **108**, 9–1 to 9–10.

- Boulanger, J.-P. & Menkes, C. 1995 Propagation and reflection of long equatorial waves in the Pacific Ocean during the 1992–1993 El Niño. *J. Geophysical Research*, **100**(C12), 25,041–25,059.
- Capotondi, A., Wittenberg, A. & Masina, S. 2006 Spatial and temporal structure of tropical Pacific interannual variability in 20th century coupled simulations. *Ocean Modelling*, **15**, 274–298.
- Collins, M. & The CMIP Modeling Groups 2005 El Niño- or La Niña-like climate change? *Clim. Dyn.*, **24**, 89–104.
- Collins, M. *et al.* 2010 The impact of global warming on the tropical Pacific Ocean and El Niño. *Nature Geosciences*, **3**. (doi:10.1038/NGEO868)
- Dewitte, B., Cibot, C., Périgaud, C., An, S.-I. & Terray, L. 2007 Interaction between near-annual and ENSO modes in a CGCM simulation: role of equatorial background mean state. *J. Climate*, **20**, 1035–1052.
- Dijkstra, H. A. 2000 *Nonlinear physical oceanography*. Kluwer Academic Publishers.
- Guilyardi, E., Braconnot, P., Li, T., Jin, F.-F., Kim, P., Kolasinski, M. & Musat, I. 2009a Mechanisms for ENSO suppression in a coupled GCM with a modified atmospheric convection scheme. *J. Climate*, **22**, 5698–5718.
- Guilyardi, E., Wittenberg, A., Fedorov, A., Collins, M., Wang, C., Capotondi, A., van Oldenborgh, G. J. & Stockdale, T. 2009b Understanding El Niño in ocean-atmosphere general circulation models. *BAMS*, pp. 325–340.
- Jin, F.-F. 1997 An equatorial ocean recharge paradigm for ENSO. Part I: conceptual model. *J. Atmos. Sci.*, **54**, 811–829.
- Large, W. G., Morzel, J. & Crawford, G. B. 1995 Accounting for surface wave distortion of the marine wind profile in low-level ocean storms wind measurements. *J. Physical Oceanography*, **25**, 2959–2971.
- Lloyd, J., Guilyardi, E., Weller, H. & Slingo, J. 2009 The role of atmosphere feedbacks during ENSO in the CMIP3 models. *Atmos. Sci. Lett.*, **10**, 170–176.
- MacMynowski, D. G. & Tziperman, E. 2010 Testing and improving enso models by process using transfer functions. *Geophys. Res. Lett.*, **37**, L19701, doi:10.1029/2010GL044050.
- McPhaden, M. J., Busalacchi, A. J., Cheney, R., Donguy, J. R., Gage, K. S., Halpern, D., Ji, M., Julian, P., Meyers, G. *et al.* 1998 The tropical ocean global atmosphere observing system: A decade of progress. *J. Geophys. Res.*, **103**(C7), 14 169–14 240.
- Meehl, G., Stocker, T., Collins, W., Friedlingstein, P., Gaye, A., Gregory, J., Kitoh, A., Knutti, R., Murphy, J. *et al.* 2007 Global climate projections. In *Climate change 2007: The physical science basis. contribution of working group I to the fourth assessment report of the intergovernmental panel on climate change* (eds S. Solomon, D. Qin, M. Manning, Z. Chen, M. Marquis, K. Averyt, M. Tignor & H. Miller). Cambridge University Press, Cambridge, United Kingdom and New York, NY, USA.

- Otto-Bliesner, B. L., Hewitt, C. D., Marchitto, T. M., Brady, E., Abe-Ouchi, A., Crucifix, M., Murakami, S. & Weber, S. L. 2007 Last glacial maximum ocean thermohaline circulation: Pmip2 model intercomparisons and data constraints. *GEOPHYSICAL RESEARCH LETTERS*, **34**(12). (doi:10.1029/2007GL029475)
- Suarez, M. J. & Schopf, P. S. 1988 A delayed action oscillator for ENSO. *J. Atmos. Sci.*, **45**, 3283–7.
- Swanson, D. C. 2000 *Signal processing for intelligent sensor systems*. CRC Press.
- van Oldenborgh, G. J., Philip, S. Y. & Collins, M. 2005 El Niño in a changing climate: a multi-model study. *Ocean Science*, **1**, 81–95.
- Wang, C. & Picaut, J. 2004 Understanding ENSO physics – a review. In *Earth's Climate: the ocean-atmosphere interaction* (ed. Wang, C and Xie, SP and Carton, JA), vol. 147 of *Geophysical monograph series*, pp. 21–48. Amer Geophys Union. Conference on Ocean-Atmosphere Interaction and Climate Variability, San Francisco, CA, DEC, 2002.
- Weisberg, R. H. & Wang, C. 1997 A western Pacific oscillator paradigm for the El Niño-Southern Oscillation. *Geophys. Res. Lett.*, **24**, 779–782.
- Welch, P. D. 1967 The use of Fast Fourier Transform for the estimation of power spectra: A method based on time averaging over short, modified periodograms. *IEEE Trans. Audio and Electroacoust.*, **AU-15**, 70–73.
- Wittenberg, A. 2009 Are historical records sufficient to constrain ENSO simulations? *Geophys. Res. Lett.*, **36**, L12 702. (doi:10.1029/2009GL038710)
- Wittenberg, A. T. 2002 Enso response to altered climates. Ph.D. thesis, Princeton University. 475pp.
- Wittenberg, A. T., Rosati, A., Lau, N. C. & Ploshay, J. J. 2006 GFDL's CM2 global coupled climate models. Part III: Tropical Pacific climate and ENSO. *J. Climate*, **19**(5), 698–722.
- Zebiak, S. E. & Cane, M. A. 1987 A model El Niño-Southern Oscillation. *Mon. Weath. Rev.*, **115**, 2262–2278.
- Zelle, H., Appeldoorn, G., Burgers, G. & van Oldenborgh, G. J. 2004 The relationship between sea surface temperature and thermocline depth in the eastern equatorial Pacific. *J. Physical Oceanography*, **34**, 643–655.